Size-Dependent Optical Absorption of Layered MoS_2 and DNA Oligonucleotides Induced Dispersion Behavior for Label-Free Detection of Single-Nucleotide Polymorphism

Bang Lin Li, Hao Lin Zou, Lu Lu, Yu Yang, Jing Lei Lei, Hong Qun Luo, and Nian Bing Li**

Size-dependent optical absorption of semiconductive (2H) layered molybdenum disulfide (MoS_2), exhibiting great discrimination abilities to single- and double-stranded DNA (ssDNA) and (dsDNA), is studied. In the presence of high concentration of salt, layered MoS_2 trends to aggregate rapidly, leading to the increases of sizes in both vertical and lateral dimensions of the nanosheets, which results from the interplay between van der Waals attraction and electrical double-layer repulsion. Meanwhile, the aggregation behavior of layered MoS_2 is remarkably inhibited by the synergistic effects of DNA oligonucleotides. ssDNA can adsorb on the surface of layered MoS_2, resulting in a great dispersion, even in the presence of high concentration of salt, while the dispersion behavior is weakened when ssDNA is replaced by dsDNA. Whereas compared to graphene with zero bandgap energy, layered MoS_2, with semiconductive properties, exhibits great characteristic optical absorption in visible wavelength region devoted to exploring the aggregation behavior of layered MoS_2. Therefore, DNA oligonucleotides induced size control of layered MoS_2, contributing to the regular change of its characteristic absorption in visible region, is considered a label-free bioassay for the detection of single-nucleotide polymorphism. Due to its easy operation and high specificity, it is expected that the proposed assay holds great promise for further applications.

1. Introduction

Recent developments in fabrication of ultrathin-layered materials down to unit cell thickness (monolayers) have enabled explorations of new low-dimensional physics, as exemplified by massless Dirac fermions and anomalous quantum Hall effects observed from 2D graphene.[1] With the penetration of graphene-related research, 2D layered inorganic materials, such as monolayer and few-layer nanosheets of molybdenum disulfide (MoS_2), hexagonal boron nitride (h-BN), and other transition metal dichalcogenides (TMDs), have attracted an increasing amount of attention.[2] While compared to graphene, with its zero bandgap energy, layered MoS_2, with its large intrinsic bandgap, shows great promise for relevant applications and also opens up new prospects for technological breakthroughs.[3]

Nanomaterials have been regarded as novel biosensing platforms due to their unique and excellent optical, electronic, and catalytic properties.[4] The developed fluorimetric sensors based on nanomaterials are becoming increasingly popular because of their inherent advantages.[2c,5] Such nanomaterials-based systems usually contain a fluorophore-labeled probe and a quencher to form a Förster resonance energy transfer pair, in which the distance-dependent fluorescence quenching is closely coupled with the biomolecular recognition event. Recently, the studied nanomaterials, mainly including graphene oxide (GO),[4a] gold nanoparticles (Au NPs),[4b,6] carbon nanotubes (CNTs),[7] and quantum dots [8] with different sizes, morphologies, and compositions, were used as highly efficient nanoquenchers to develop novel fluorimetric sensors. These nanomaterials also exhibited great discrimination abilities to single- and double-stranded DNA (ssDNA) and (dsDNA) because of series of external forces. More recently, layered MoS_2 was also found to be a good nanoquencher and adopted as a new platform to construct biosensor based on its intrinsic discrimination abilities to ssDNA and dsDNA, showing the similar property and application with graphene.[2c] However, we noticed that the wide applicaions of nanomaterials-based fluorimetric sensors were limited due to the drawback that the fluorophore-labeled method made those assays complex, high-cost, and time-consuming. Therefore, label-free approaches based on nanomaterials are encouraged with much more attention.[9,10]

Significantly, single- and few-layer MoS_2 have been exploited for sensors,[2b,c,11] transistors,[12] integrated circuits,[12b]

B. L. Li, H. L. Zou, L. Lu, Y. Yang, Prof. H. Q. Luo, Prof. N. B. Li
Key Laboratory of Ecoenvironments in Three Gorges Reservoir Region (Ministry of Education)
School of Chemistry and Chemical Engineering
Southwest University
Chongqing 400715, P. R. China
E-mail: luohq@swu.edu.cn; linb@swu.edu.cn
Prof. J. L. Lei
School of Chemistry and Chemical Engineering
Chongqing University
Chongqing 400044, P. R. China

DOI: 10.1002/adfm.201500180

nanometer thick photovoltaics,[13] supercapacitors,[14] and hydrogen evolution catalysis.[15] Several recent reseaches have shown bandgap tuning of MoS_2 with layer thickness, from 1.2 eV indirect bandgap for bulk crystals to a direct gap semiconductor owning a 1.9 eV bandgap for a single-layer MoS_2. The exceptional electronic and optical properties of the layered semiconductor nanomaterials inject new opportunities in the field of photonics, optoelectronics, and other kinds of applications.[16] Meanwhile, we noticed that the strong absorption and photoluminescence bands of single- and few-layer MoS_2 were also observed in the visible wavelength region, which were strongly influenced by varying the plane size and thickness of the nanosheets due to their unique electronic and optical properities.[17] Therefore, the optical properties of layered MoS_2, exhibiting a considerable quantum-confinement effect that is visible in its absorption spectrum, could provide great challenges for layered MoS_2 applications in bioanalysis. Given that the aggregation of individual nanomaterial always resulted in the change of microstructure of nanomaterials, we found that layered MoS_2, without any protection, trended to aggregate with the acceleration of salt-induced effect, shown in its characteristic absorption spectrum. Nevertheless, ssDNA could adsorb on the surface of layered MoS_2, resulting in a great dispersion, even in the presence of optimized concentration of salt. The DNA oligonucleotides induced dispersion behavior was remarkably weakened when the original ssDNA was replaced by same concentration of dsDNA. Therefore, taking advantage of the size-dependent absorption of layered MoS_2 and intrinsic discrimination abilities to ssDNA and dsDNA, DNA oligonucleotides induced size control of layered MoS_2 in aqueous salt solution, contributing to the regular change of its characteristic absorption in the visible region, was considered a new bioassay to construct the detection of target ssDNA. Finally, the proposed bioassay was also devoted to the detection of single-nucleotide polymorphism (SNPs) based on the unique and great properties of layered MoS_2.

2. Results and Discussion

2.1. Characteristic Absorption of Layered MoS_2

Ultrasonic waves generate cavitation bubbles that collapse into high-energy jets, apparently breaking up the layered crystallites and producing exfoliated nanosheets.[2d,18] Therefore, up to now, graphene,[18a] layered h-BN, 2D TMDs s have already been obtained in that proposed approach,[18b] showing great promise in further applications. In our experiments, few-layer MoS_2 nanosheets were prepared by exposing bulk MoS_2 crystals to ultrasonic waves in an aqueous sodium cholate solution, which was first mentioned by Coleman and co-workers.[19] A number of layered crystals can be exfoliated in water, resulting in thin flakes stabilized by a surfactant coating. This method is robust, can be carried out in ambient conditions, is scalable, and allows the preparation of films, hybrids, and composites.[19] In the beginning, MoS_2 crystals were added to sodium cholate aqueous solution for sonication treatment, resulting in a black dispersed solution (**Figure 1**A). Subsequently, centrifugation

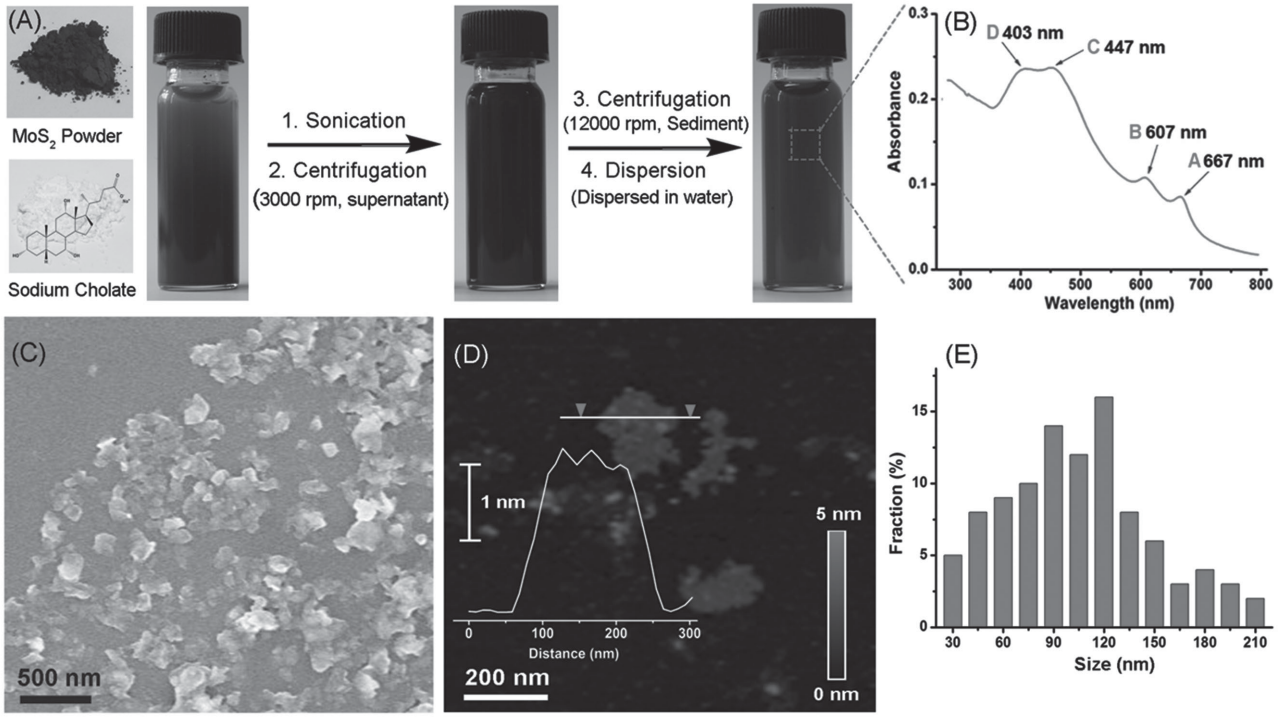

Figure 1. A) Photographs of the MoS_2 dispersions being processed at different stages. B) Optical absorption spectrum of layered MoS_2 aqueous solution. C) SEM and D) AFM images of as-exfoliated layered MoS_2 with the inset representing the height profile along the white line overlaid on the image. E) The plane size distribution based on 100 randomly selected few-layer MoS_2 nanosheets.

of the dispersion at 3000 rpm and collection of yellow–green supernatant were used to remove the bulk and thicker MoS_2. The precipitation was then collected at 12 000 rpm to obtain as-exfoliated layered MoS_2 nanosheets. Furthermore, the surfactant adsorbed on the surface of layered MoS_2 was removed through redispersal of the sediments in ultrapure water with the assistance of ultrasonication and collection of the new sediments at 12 000 rpm, which was verified using thermogravimetric analysis in our previous report.[20] Whereas bulk MoS_2 is a semiconductor with an indirect bandgap of 1.3 eV, single-, double-, and triple-layer MoS_2 is direct-gap semiconductors with bandgaps of 1.8, 1.65, and 1.35 eV, respectively, and strong absorption can be observed in as-exfoliated layered MoS_2 nan osheets.[17a,c,21,22] As is shown in Figure 1A, the layered MoS_2 aqueous dispersion appears to be yellow–green in color and the detailed optical property of the layered MoS_2 is studied by measuring its optical absorption spectrum (Figure 1B). The four characteristic absorption peaks located at 600–700 and 400–500 nm regions coincide with the general features of TMDs with trigonal prismatic coordination, implying the layered MoS_2 2H polytype.[17c,23] The absorption peaks correspond to four kinds of electronic transitions, termed A, B, C, and D, in the band structure of MoS_2. The former, dual peaks at 667 nm (1.859 eV) and 607 nm (2.043 eV), derived from A and B, the interband excitonic transitions at the K point of the Brillouin zone in 2D MoS_2 with large lateral dimensions.[17c,23,24] The splitting of valence bands is due to the combined effect of interlayer coupling and spin–orbit coupling.[23,24] Referring to the relationship between exciton energy of the A peak and the thickness of the layered MoS_2, it is estimated that the average thickness of the nanosheets in MoS_2 dispersions is close to be 4 nm,[25] which is consistent with the statistical result in our previous reports.[20,26] In addition to the two broad peaks centered at 447 nm (C exciton) and 403 nm (D exciton), it has been suggested that the optical absorption of low-dimensional MoS_2 exhibits a strong blueshift when the plane size of the MoS_2 nanostructures is reduced to less than 50 nm, ascribed to the quantum size effect.[17c] Furthermore, the optical absorption stability of the layered MoS_2 aqueous solution was discussed and the result is shown in Figure S1 (Supporting Information). It was found that the layered MoS_2 aqueous solution exhibited great optical absorption stability when the standing time was less than 8 h. With increasing standing time (>12 h), the absorbance of dispersion trended to decrease due to the slow aggregation of layered MoS_2 with the influence of Van der Waals interaction between nanosheets. However, the absorbance of aggregated layered MoS_2 recovered to the original value with the assistance of sonication treatment for 2 min.

The sheet structure and morphology are shown on the scanning electron microscope (SEM) image (Figure 1C), primarily showing the nanoscale of as-exfoliated MoS_2 with plane size of around 120 nm. It was reported that the thickness of layered MoS_2, obtained from sonication-assisted exfoliation, was inhomogeneous ranging from mono-layer to few-layer.[18,19] The atomic force microscope (AFM) image of as-prepared layered MoS_2 is shown in Figure 1D, wherein the thickness of layered nanosheet studied is estimated to be around 1.9 nm, corresponding to about three monolayers of MoS_2.[2b] Statistical analysis (shown in Figure 1E) based on SEM and AFM measurements indicated that the layered MoS_2 prepared from the sonication-assisted exfoliation technique had various plane sizes ranging from 30 to 210 nm, with the majority of 90–120 nm, corresponding to the analysis results of four exciton peaks in optical absorption spectrum (Figure 1B). Furthermore, the Raman and photoluminescence (PL) spectra of as-exfoliated layered MoS_2 were recorded. As shown in Figure S2 (Supporting Information), the characteristic bands at 379.04 and 403.12 cm^{-1} are assigned as the in-plane vibration (E^1_{2g}) of two atoms with respect to the Mo atom and out-of-plane (A_{1g}) vibration of S atoms. the frequency difference of the two modes can be used to distinguish the layered MoS_2 and its bulk counterpart.[27] A mean frequency difference of 24.08 cm^{-1} was obtained for the few-layer nanosheets, while the value for the bulk MoS_2 was increased to 25.98 cm^{-1}. Therefore, it was demonstrated that the Raman spectra of layered MoS_2 exhibit the distinct Raman fingerprint of the 2H-MoS_2 crystal with no evidence of structural distortion.[27] The PL spectrum (Figure S2, Supporting Information) of layered MoS_2 contains two peaks at about 681 and 627 nm, corresponding to the direct excitonic transitions between the minimum of the conduction band and the maxima of split valence bands.[1]

2.2. Salt-Induced Aggregation of Layered MoS_2

Salt-induced aggregation behaviors of nanomaterials, including graphene composite,[9] GO,[28] AuNPs,[29] CNTs,[30] and polymer nanoparticles,[31] were studied, showing great properties for a range of applications. In our experiment, the behavior of layered MoS_2 was studied in the presence of high concentration of Na^+ ions using absorption spectra. From **Figure 2**A, it is observed that with the addition of 100×10^{-3} M NaCl, the absorbance of layered MoS_2 dispersion peaked at 667 (A exciton) and 607 nm (B exciton) increases in a short time. Meanwhile, the locations of those two peaks also shift to the red wavelength, correspondingly, whereas the broad absorption of convoluted C and D excitonic peaks between 400 and 450 nm decreases. It was reported that the location of A excitonic peak was associated with the average thickness of layered MoS_2, namely, the number of layers.[25] The located wavelength of A absorption peak increased as a consequence of the increases of vertical dimensional thickness of layered MoS_2. Therefore, it was estimated that the energy of characteristic A exciton peak decreased from 1.859 eV to 1.845 eV within 30 min (Figure 2B), corresponding to the increase of average thickness of layered MoS_2 from about 4 nm to more than 8 nm. The results show that the aggregation of layered MoS_2 occurs with the addition of high concentration of NaCl. Meanwhile, the remarkable increases of absorbance of A and B excitonic peaks (Figure 2A and inset of Figure 2B), followed by the decreases of absorbance of broad C and D excitonic peaks (Figure 2A and Figure S3, Supporting Information), show that a number of low-dimensional or quantum dots MoS_2 (<50 nm) trend to aggregate forming the larger one in its lateral dimension.[17c] That is to say, salt-induced aggregation of layered MoS_2 leads to the increase of sizes in both vertical and lateral dimensions within a short time, forming aggregated layered MoS_2 (Figure 2C). In order to confirm the deduction, the

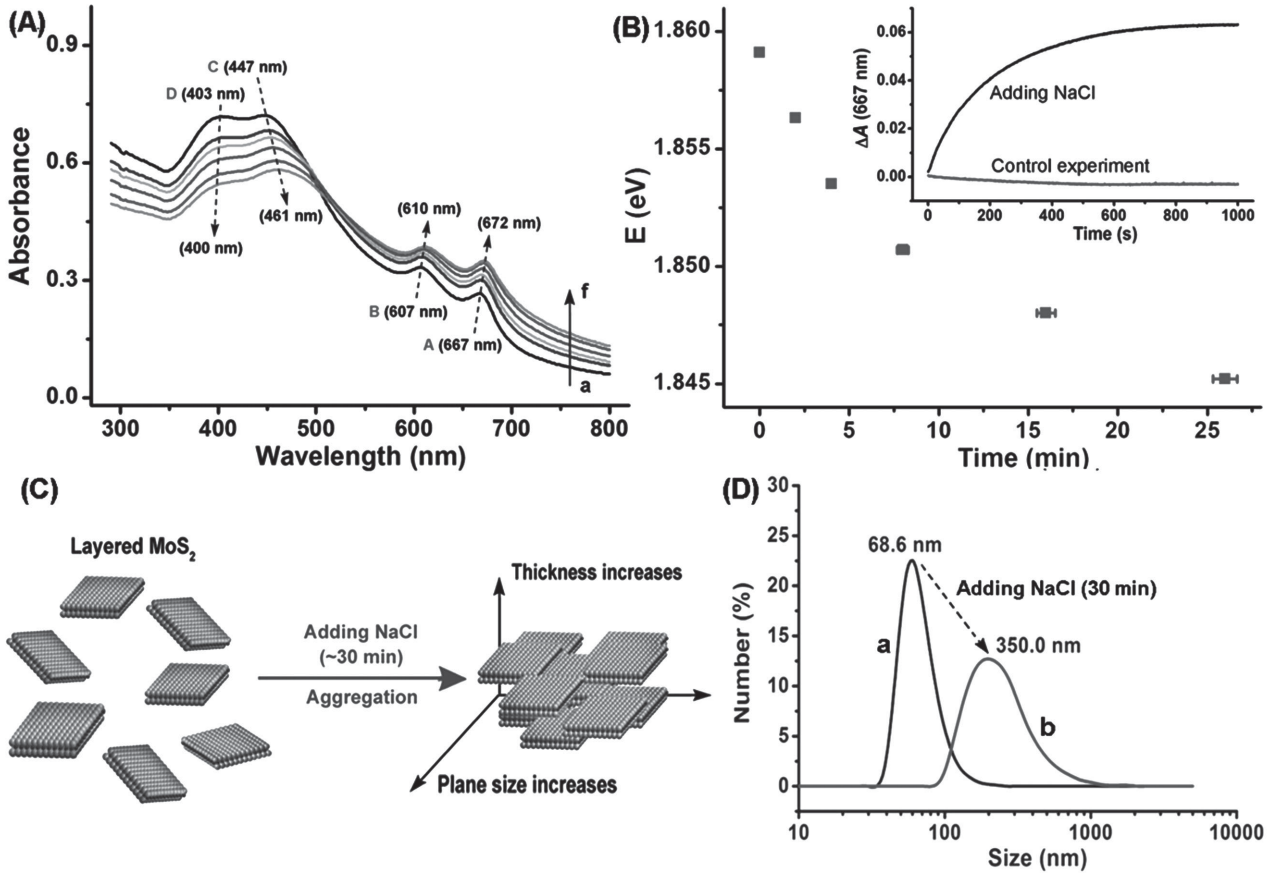

Figure 2. A) Optical absorption spectra of layered MoS_2 dispersion a) before and after adding 100×10^{-3} M NaCl for various standing times (b: 2 min; c: 4 min; d: 8 min; e: 16 min; f: 26 min). B) The energy of the A exciton peak as a function of standing time and the inset shows the time-dependent absorbance of layered MoS_2 dispersion at wavelength of 667 nm in the absence and presence of 100×10^{-3} M NaCl. ΔA represents the change of absorbance of layered MoS_2 dispersion. C) The scheme illustration of aggregation of layered MoS_2 in aqueous NaCl solution. D) Hydrodynamic size distributions of layered MoS_2 a) before and b) after addition of NaCl for 30 min measured by DLS.

AFM image of aggregated layered MoS_2 was recorded and is shown in Figure S4 (Supporting Information). From Figure S4 (Supporting Information), MoS_2 nanosheets with plane size of around 400 nm and vertical size of over 10 nm are observed, which are larger than that of layered MoS_2 before the addition of NaCl. The result was also demonstrated using dynamic light scattering (DLS) measurements. A fourfold increase in average size of layered MoS_2 is observed after the addition of 100×10^{-3} M NaCl for 30 min (Figure 2D), corresponding to the aggregation behavior of as-prepared layered MoS_2.

The crystal structure of the aggregated layered MoS_2 was investigated in detail. From the X-ray diffraction (XRD) pattern shown in Figure S5 (Supporting Information), it can be observed that both layered MoS_2 and aggregated layered MoS_2 are identified as semiconducting (2H) MoS_2 with a dominant peak appearing at 14.4°, representing the (002) plane (ICDD card no. 77-1716). MoS_2 has two different types of phases, i.e., stable hexagonal 2H phase and metastable metallic (1T) phase, where it has been demonstrated that a transition from 2H to 1T phase occurs after the semiconducting MoS_2 was intercalated with Li^+, K^+, Na^+, and H^+. To explore the phase type of layered MoS_2 with the influence of salt-induced aggregation, high resolution Mo 3d and S 2p spectra of aggregated layered MoS_2 were recorded (Figure S6, Supporting Information). Mo $3d_{3/2}$, Mo $3d_{5/2}$, S $2p_{1/2}$, and S $2p_{3/2}$ peaks were observed at 232.8, 229.6, 163.7, and 162.5 eV, respectively, showing the dominant 2H phase. Meanwhile, no 1T phase peaks were found. Therefore, it was demonstrated that the original semiconducting phase (2H) of as-exfoliated MoS_2 was not influenced by Na^+-induced aggregation behavior.

The monovalent cation (Na^+) should have no specific interaction with the surface of layered MoS_2. The aggregation of layered MoS_2 in the presence of Na^+ can thus be explained by the charge screening theory that separation of every subsequent proton from the nanosheets surfaces in the electrolyte is resisted by the electric field created by "free" ions in the solution. An increasing amount of added electrolyte can thus provide additional shielding to the charge surface to reduce the electric repulsive forces between nanosheets and then promote their aggregation.[32] However, with the increase of standing times (>30 min), the concentration of small layered MoS_2 becomes low and the aggregation behavior of layered MoS_2 is weakened. No red shift can be observed in location of A excitonic peak in absorption spectra of layered MoS_2 dispersion

in this further process (Figure S7, Supporting Information). Nevertheless, we found that the absorbance of A, B, C, and D excionic peaks decreased, which could be ascribed to that salt-induced aggregation phenomenon resulted in the decrease of dispersity of layered MoS_2 aqueous solution and the sedimentation of aggregated layered MoS_2 began to occur, subsequently.

2.3. Sedimentation Behavior of Aggregated Layered MoS_2

The sedimentation behavior of aggregated layered MoS_2 was studied using A and B excitonic peaks, which represented the characteristic absorption of layered MoS_2 with 2D scale.[17c] In the presence of high concentration of NaCl, sedimentation phenomenon of layered MoS_2 occurred rapidly. The absorption spectra of supernatant derived from the top two-thirds of the dispersion were measured at various standing times. From **Figure 3**A, it is observed that the absorbance of layered MoS_2 decreases with increasing standing times and those characteristic absorption peaks almost disappear when the standing time is close to 8 h. The time-dependent absorbance of layered MoS_2 dispersion was recorded in the absence and presence of different concentrations of NaCl. From Figure 3B, we find that the sedimentation of layered MoS_2 is influenced by the concentration of salt. When the concentration of NaCl is over 10×10^{-3} M, the sedimentation of layered MoS_2 occurs much more rapidly. In order to account for sedimentation behavior of layered nanosheets, the sedimentation experiments of layered MoS_2 in the presence of different kinds of electrolyte solutions (NaCl, $CaCl_2$, and $AlCl_3$) were first studied using absorption spectra. It is observed that the sedimentation behaviors of MoS_2 nanosheets in different kinds of salt solutions are distinguished (Figure S8, Supporting Information), which can be explored using the Schulze–Hardy rule:

$$\log(\text{ccc}) \approx n \log\left(\frac{1}{z}\right) \quad (1)$$

where z is the valency of the electrolyte counterions and ccc, known as the critical coagulation concentration, represents the minimum concentration of ions necessary to cause rapid coagulation of colloids. Typically, n is 6 in 3D and 9 in 2D.[9] The coagulation curve for layered MoS_2 in aqueous solution as a function of NaCl concentration was recorded in **Figure 4**A. The concentration of layered MoS_2 versus NaCl concentration almost remained constant until it obviously decreased with the concentration of NaCl exceeding a threshold value. When the normalized layered MoS_2 concentration became 0.5, the real-time NaCl concentration was regarded as the ccc of Na^+ for layered MoS_2. Similarly, coagulation curves for Ca^{2+} and Al^{3+} were recorded in Figure 4B,C, respectively. The corresponding ccc values for all ions are summarized in **Table 1**. In accordance with the Schulze–Hardy rule, the double-logarithmically plot of ccc for different kinds of ions against the ionic valence was recorded in Figure 4D. The slope of this line was estimated to be around 8.08, which was close to 9. Therefore, it was demonstrated that the layered MoS_2 dispersion followed the 2D Schulze–Hardy rule, which was ascribed to the interplay between van der Waals attraction and electric double-layer repulsion.

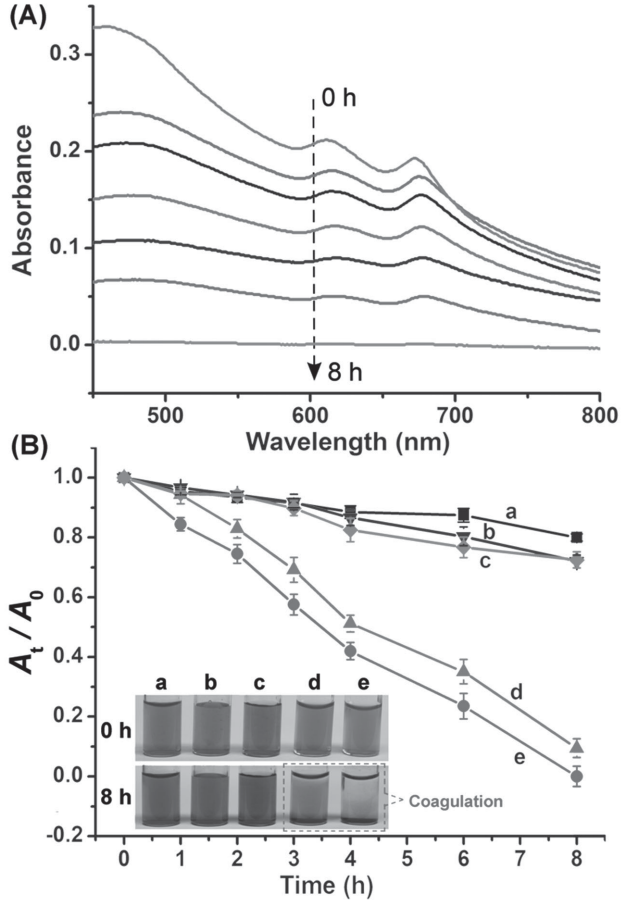

Figure 3. A) Absorption spectra of aqueous layered MoS_2 solution in the presence of 100×10^{-3} M NaCl with various standing times from 0 to 8 h. B) Time-dependent absorbance of aqueous layered MoS_2 solution in the a) absence and b–e) presence of various concentrations of NaCl (b: 0.1×10^{-3} M; c: 1.0×10^{-3} M; d: 10.0×10^{-3} M; e: 100.0×10^{-3} M). A_0 and A_t represent the absorbance (672 nm) of layered MoS_2 dispersion before and after different standing times.

2.4. Discrimination Abilities of Layered MoS_2

Single-layer MoS_2 can be viewed as an "S-Mo-S" sandwich structure, stacking a positively charged molybdenum plane between two negatively charged sulfur planes. In the previous report, it was first demonstrated that layered MoS_2, obtained from the electrochemical lithium-intercalation method, could adsorb dye-labeled ssDNA probe via the van der Waals force between nucleobases and the basal plane of MoS_2 and then quenched the fluorescence of the dye. Nevertheless, when the ssDNA probe was hybridized with its complementary target DNA, as the nucleobases were buried between the densely negatively charged helical phosphate backbones, the interaction between the formed dsDNA and layered MoS_2 was weakened, resulting in that the dye-labeled probe was away from layered MoS_2 and thus the fluorescence of the probe retains.[2c] More recently,

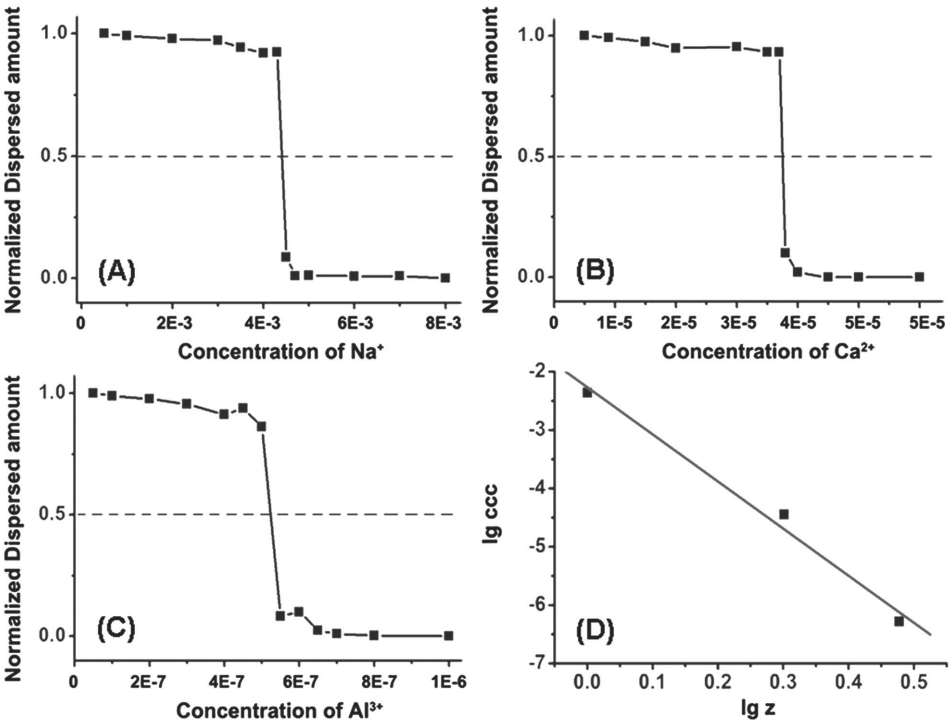

Figure 4. Normalized concentration of layered MoS_2 against A) NaCl, B) $CaCl_2$, and C) $AlCl_3$ concentrations. D) Double-logarithmic plot of the critical coagulation concentration against the ionic valency. The solid line has a slope of −8.08.

few-layer MoS_2 nanoflakes were also reported to own differential affinity toward ssDNA and dsDNA, which were used for DNA hybridization detection based on their inherent electrochemical activity.[33] On the basis of the above works, the affinity experiment of as-obtained layered MoS_2 to DNA was designed to verify its discrimination abilities. In our experiments, layered MoS_2 was added to fluorescein-labeled probe ssDNA (FAM-T1) and it is observed from Figure S9 (Supporting Information) that the fluorescence of FAM-T1 is quenched effectively, suggesting that the interaction between ssDNA and as-prepared layered MoS_2 is quite strong. However, after FAM-T1 has been hybridized with an equal amount of the complementary target ssDNA (T2) to form dsDNA, the fluorescence of T1/T2 duplex is obviously retained. The fluorescence of T1/T2 duplex in the absence of layered MoS_2 is observed to slightly decrease when compared to FAM-T1, which can be ascribed to the effect of primary and secondary structure of DNA on the fluorescence properties of labeled dyes. Therefore, we can conclude that the layered MoS_2, obtained from sonication-assisted exfoliated of bulk MoS_2 in aqueous surfactant solution, exhibits a higher affinity to ssDNA than dsDNA, showing great discrimination abilities.

Table 1. Critical coagulation concentrations (ccc) of layered MoS_2 for various ions in aqueous solutions.

Ions	Na^+	Ca^{2+}	Al^{3+}
ccc [$\times 10^{-3}$ M]	4.4	0.036	0.00053

2.5. DNA Oligonucleotides Induced Dispersion Behavior

It was demonstrated that the ssDNA could stably adsorb on layered MoS_2, due to the strong van der Waals interaction between the ring structure in the nucleobases and the surface of nanosheets. Furthermore, when a certain amount of label-free ssDNA T1 was added to the layered MoS_2 to form layered MoS_2/T1 complex, the salt-induced aggregation phenomenon of original layered MoS_2 was inhibited, regularly, which could be ascribed to that the negatively charged DNA backbone on the surface of layered MoS_2 increased individual nanosheets electrostatic repulsion and thus resisted salt-induced aggregation. In the presence of optimized concentration of Na^+ (10×10^{-3} M), the coagulation of layered MoS_2/T1 complex was inhibited, corresponding to the increase of ssDNA T1 concentration (**Figure 5**A). When the concentration of T1 increased to 7.5×10^{-9}M, the coagulation of layered MoS_2 was likely to be highly inhibited and the result is shown in its absorbance of both characteristic A and B excitonic peaks (Figure 5B). Nevertheless, dsDNA cannot stably adsorb on layered MoS_2 because the ring structure of nucleobases is effectively shielded within the densely negatively charged phosphate backbone of dsDNA, and thus the addition of dsDNA cannot inhibit the coagulation of layered MoS_2 in salt solution. The proposed idea was verified using absorption spectrum. In our designed experiment, label-free probe T1 can be hybridized with complementary target ssDNA T2 to form T1/T2 duplex (Figure 5C). When compared to the absorption spectrum of layered MoS_2 protected by ssDNA T1 (curve c, Figure 5D), the decreases of characteristic A and B peaks absorbance were observed in that of

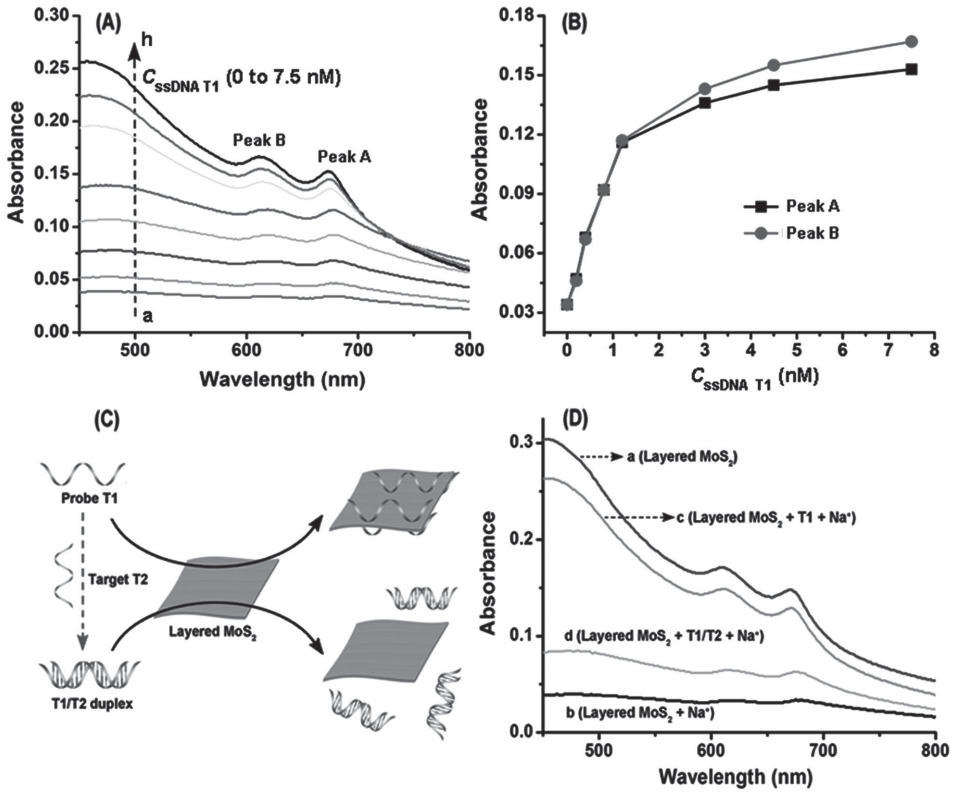

Figure 5. A) Optical absorption spectra of layered MoS_2 in the a) absence and b–h) presence of different concentrations of ssDNA T1 (b: 0.2; c: 0.5; d: 0.8; e: 1.2; f: 3.0: g: 4.5; h: 7.5×10^{-9} M) with the addition of 10×10^{-3} M NaCl. B) Absorbance of layered MoS_2 dispersions at peak A (672 nm) and B (610 nm) versus varying the concentration of ssDNA T1. C) Scheme of the interaction between DNA (ssDNA and dsDNA) and layered MoS_2. D) Optical absorption spectra of a) layered MoS_2 dispersed in water and layered MoS_2 dispersions in b) the absence and c) presence of probe ssDNA T1 and d) T1/T2 duplex with the addition of 10×10^{-3} M NaCl.

layered MoS_2 protected by T1/T2 duplex (curve d, Figure 5D), showing a weaker inhibition effect of dsDNA to the coagulation of layered MoS_2 in the presence of optimized concentration of Na^+ ion.

2.6. Sensor Applications

Herein, a new approach to distinguish ssDNA and dsDNA was proposed based on the signal of characteristic optical absorption of layered MoS_2. On the basis of the proposed approach, we developed a label-free colorimetric detection method for DNA sequence specificity combining the distinguished influence of ssDNA and dsDNA to the inhibition of coagulation of layered MoS_2. The protocol of our method is shown in **Figure 6**A. Meanwhile, a portion of supernatant (700 µL) was separated to measure the absorbance using an optical absorption spectrophotomer (Figure 6B), corresponding to the detection of target DNA (T2). From **Figure 7**A, it is found that the absorbance (672 nm) of layered MoS_2 decreased linearly with increasing concentration of T2 from 0.5 to 7.5×10^{-9} M and the linear regression equation for target DNA was $A = 0.1495–0.0187$ C (C: $\times 10^{-9}$ M). Meanwhile, the detection limit, defined as the concentration of the analyte giving signals equivalent to three times the standard deviation of the blank signals ($S/N = 3$), was estimated to be 0.315×10^{-9} M. It should be highlighted that the relative standard deviation values shown in the calibration plot are lower than 6%, suggesting good reproducibility. Furthermore, this developed DNA sensor could be used to differentiate single mismatches, providing the opportunity to detect SNPs. As is shown in Figure 7B, the absorbance change for the single mismatched duplex DNA (M1, M2, or M3, respectively) is obviously different when compared to that of complementary duplex DNA (T1/T2). The high sequence specificity for single mismatches was quite impressive, indicating that this developed bioassay should exhibit great promise in further applications. The method based on optical absorption spectrum is low-cost, simple, and highly sensitive. Nevertheless, compared with other methods based on functionalized nanomaterials, such as CNT, graphene, Au nanoparticles, and quantum dots, the developed sensor was simple and reliable, because layered MoS_2 was used without functionalization and the absorption responses were directly provided by the 2D nanosheets. 2D layered MoS_2 as a direct bandgap semiconductor with characteristic optical absorption should own wide applications in fabrications of electronic devices, and the potential of layered MoS_2 in biosensors also needs to be exploited with more attention.

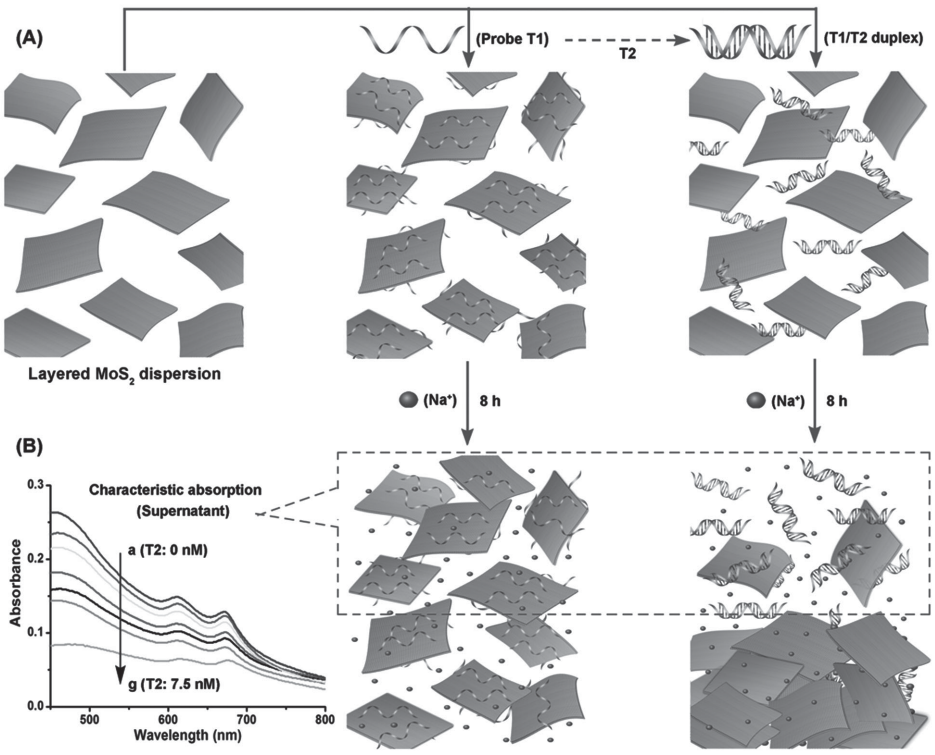

Figure 6. A) The scheme illustration of label-free DNA biosensor based on ssDNA induced dispersion behavior of layered MoS_2 in aqueous salt solution. B) Absorption spectra of layered MoS_2 (700 μL of the supernatant) in the presence of different amounts of T2 (from 0 to 7.5×10^{-9} M) with the fixed concentration of T1 (7.5×10^{-9} M).

3. Conclusion

In summary, layered MoS_2, obtained from sonication-assisted exfoliation of bulk crystals in aqueous surfactant solution, exhibited great discrimination abilities to ssDNA and dsDNA. The aggregation and sedimentation behavior of layered MoS_2 in aqueous salt solutions was studied based on its characteristic optical absorption. It was demonstrated that salt-induced aggregation of layered MoS_2 resulted in the increase of sizes in both vertical and lateral dimensions of the 2D nanomaterial, and then the sedimentation behavior of aggregated layered MoS_2 occurred, subsequently. Furthermore, ssDNA was found to be adsorbed on the surface of layered MoS_2 and inhibit the coagulation of layered MoS_2. In contrast, dsDNA stayed away from the surface of layered MoS_2 and thus the inhibition effect was weakened. On the basis of the characteristic optical absorption of layered MoS_2, a new platform for DNA detection was developed combining the discrimination abilities of layered MoS_2 to ssDNA and dsDNA, and ssDNA induced dispersion behavior of these nanosheets. Significantly, the direct application of size-dependent optical absorption properties of layered MoS_2 makes the construction of label-free biosensors possible, which is more advantageous, simpler, and cheaper than the previous method based on fluorescein-labeled probe ssDNA. Furthermore, the developed bioassay was devoted to detection of SNPs with a satisfactory result. The characteristic absorption of layered MoS_2 was first used to the developments of biosensors. The use of 2D TMDs such as layered MoS_2 for the developments of sensors and biosensors is a recent research field with great potential.

4. Experimental Section

Materials: Molybdenum sulfide (MoS_2 crystalline powder, <2 μm, 99%) was purchased from Sigma-Aldrich Co. (USA). Sodium cholate (98%) and 2-amino-2-(hydroxymethyl)-1,3-propanediol (tris) were obtained from Aladdin Chemistry Co., Ltd. (Shanghai, China). All electrolytes (NaCl, $CaCl_2$, and $AlCl_3$) were purchased from Kelong Chemical Reagent Co., Ltd. (Chengdu, China). DNA oligonucleotides were purchased from Sangon, Inc. (Shanghai, China), and used as received: probe DNA (T1), 5′-GCAGACACATCCAGCGATAGCCAGGACAA-3′; FAM-labeled probe DNA (FAM-T1), 5′-FAM- GCAGACACATCCAGCGATAGCCAGGACAA-3′; wild-type hepatitis B virus (HBV) DNA (T2), 5′-TTGTCCTGGCT-ATCGCTGGATGTGTCTGC-3′; single mismatch mutated HBV DNA (M1), 5′-TTGTCCTGGCTATCTCTGGATGTGTCTGC-3′; single mismatch mutated HBV DNA (M2), 5′-TTGTCCTGGCTATCACTGGATGTGTCTGC-3′; single mismatch mutated HBV DNA (M3), 5′-TTGTCCTGGCT-ATCCCTGGATGTGTCTGC-3′. Other chemicals were of analytical reagent grade and used without further purification. Ultrapure water (18.2 MΩ cm) was used throughout the experiment.

Experimental Instrumentations: The KQ-250B ultrasonic bath (250 W, Kun Shan Ultrasonic Instruments Co., Ltd., China) was used for the exfoliation of MoS_2 crystals. Optical absorption spectra were recorded on a UV-2450 UV–vis spectrophotomer (Shimadzu, Japan) at room temperature. The nanosheets morphologies of layered MoS_2 were observed using an S-4800 field-emission SEM (Hitachi, Japan)

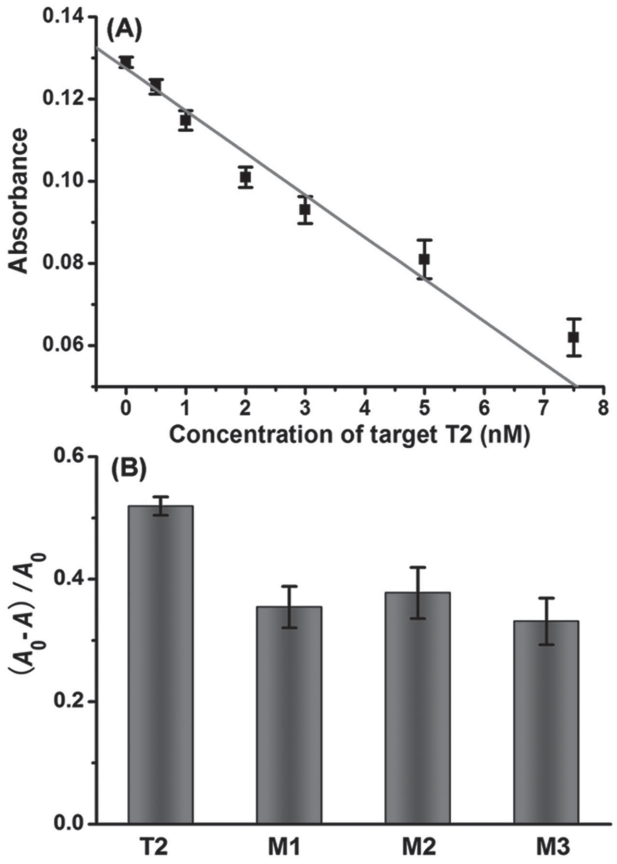

Figure 7. A) Linear relationship between the absorbance of layered MoS_2 before and after addition of various amounts of target T2 with the fixed concentration of T1 (7.5×10^{-9} M). B) The change of signal decrease percentage $(A_0 - A)/A_0$, where A_0 and A represent the absorbance of characteristic A peak (672 nm) of layered MoS_2 between complementary ssDNA T2 and single-mismatched ssDNA M1, M2, and M3, respectively.

and a dimension icon AFM (Bruker, Germany). All fluorescence (FL) spectra were recorded on an F-2700 fluorescence spectrophotometer (Hitachi, Japan). Hydrodynamic size distribution was measured on a Malvern Zetasizer Nano ZS analyzer. XRD patterns were obtained from a D8 DISCOVER X-ray diffractometer (Bruker, Germany) and X-ray photoelectron spectra (XPS) analyses were conducted using an ESCALAB 250Xi X-ray photoelectron spectroscopy (Thermo Electron, USA). Raman and photoluminescence (PL) spectra were recorded on a confocal laser Raman spectrometer (Renishaw, UK) with a excitation wavelength of 532 nm. Centrifugation was conducted using a TGL-16M high-speed refrigerated centrifuge (Xiangyi, China).

Preparation of Layered MoS_2: Layered MoS_2 was obtained through sonication-assisted exfoliation of bulk MoS_2 crystals in aqueous surfactant solution. A portion of mixed water solution, containing 5 mg mL^{-1} MoS_2 powder and 1.5 mg mL^{-1} sodium cholate, was sonicated (250 W) at normal temperature for 20 h, resulting in the preparation of black dispersion. Subsequently, the resultant dispersion was centrifuged at 3000 rpm for 30 min, followed by the separation of the yellow–green supernatant to remove bulk MoS_2. The separated supernatant was centrifuged at 12 000 rpm (30 min) for isolation of layered MoS_2. In order to remove sodium cholate adsorbed on the surface of nanosheet, the layered MoS_2 collected was dispersed in ultrapure water with the assistance of sonication. Similarly, the regenerated dispersion was centrifuged at 12 000 rpm for 30 min, followed by the collection of sediments to complete the washing process. The washing process was then repeated a further two times to remove sodium cholate completely. Ultimately, the sediments were dispersed in a certain amount of ultrapure water to prepare uniform layered MoS_2 dispersion. Furthermore, in order to obtain a high reproducibility for optical absorption detection, the stock solution of layered MoS_2 should be used after sonication-treatment for 2 min.

Determination of Critical Coagulation Concentration: Layered MoS_2 dispersions (100 μL, 0.5 mg mL^{-1}) were added to different concentrations of standard electrolytes solutions (900 μL), respectively. All electrolytes adopted were supplied as chloride salts in the form of XCl_z, where X is Na^+, Ca^{2+}, or Al^{3+}, respectively, and z represents the charge number of cation. The as-prepared dispersions were left undisturbed for 8 h at room temperature and the concentration of layered MoS_2 in the supernatant solution, derived from the top two-thirds of the dispersion, was determined by measuring the absorbance at 610 nm. Optical absorption spectra showed that the amount of material retained (characterized by $A/l = \alpha C$, where A/l is the absorbance per length, α is the extinction coefficient, and C is the concentration) could be quantitatively monitored.

DNA Bioassay: Prior to the addition of the layered MoS_2 solution, the hybridizations of probe ssDNA (T1) with different amounts of its complementary target DNA (T2) were conducted at 95 °C in buffer (800 μL, 25×10^{-3} M Tris–HAc buffer solution, pH 7.4), and the mixtures were cooled to room temperature. Then, 100 μL of as-obtained layered MoS_2 dispersion (0.5 mg mL^{-1}) was added to the mixed solution and incubated for 5 min. Subsequently, NaCl solution (100 μL) was added to the above solution to a final concentration of 10×10^{-3} M. The solution was left undisturbed for 8 h at room temperature, allowing the aggregation of layered MoS_2. Finally, a portion of supernatant (700 μL) was separated to measure the absorbance. SNPs detection was also performed based on the above procedure on hybridization of different amounts of M1 (or M2, M3) with T1. The whole detection process would last about 9 h.

Supporting Information

Supporting Information is available from the Wiley Online Library or from the author.

Acknowledgements

This work was supported by the National Natural Science Foundation of China (Nos. 20975083 and 21273174) and the Municipal Science Foundation of Chongqing City (No. CSTC2013jjB00002).

Received: January 15, 2015
Revised: April 4, 2015
Published online: May 6, 2015

[1] a) A. Splendiani, L. Sun, Y. Zhang, T. Li, J. Kim, C.-Y. Chim, G. Galli, F. Wang, *Nano Lett.* **2010**, *10*, 1271; b) Y. Liu, H. Nan, X. Wu, W. Pan, W. Wang, J. Bai, W. Zhao, L. Sun, X. Wang, Z. Ni, *ACS Nano* **2013**, *7*, 4202.

[2] a) Y. X. Yuan, R. Q. Li, Z. H. Liu, *Anal. Chem.* **2014**, *86*, 3610; b) J. Z. Ou, A. F. Chrimes, Y. C. Wang, S. Y. Tang, M. S. Strano, K. Kalantar-zadeh, *Nano Lett.* **2014**, *14*, 857; c) C. Zhu, Z. Zeng, H. Li, F. Li, C. Fan, H. Zhang, *J. Am. Chem. Soc.* **2013**, *135*, 5998; d) X. Huang, Z. Zeng, H. Zhang, *Chem. Soc. Rev.* **2013**, *42*, 1934.

[3] G. Deepesh, D. Damien, M. M. Shaijumon, *ACS Nano* **2014**, *8*, 5297.

[4] a) C. T. Lin, P. T. K. Loan, T. Y. Chen, K. K. Liu, C. H. Chen, K. H. Wei, L. J. Li, *Adv. Funct. Mater.* **2013**, *23*, 2301; b) D. B. Liu, Z. Wang, X. Y. Jiang, *Nanoscale* **2011**, *3*, 1421; c) K. P. Loh, Q. L. Bao, G. Eda, M. Chhowalla, *Nat. Chem.* **2010**, *2*, 1015.

[5] K. M. Wang, Z. W. Tang, C. Y. J. Yang, Y. M. Kim, X. H. Fang, W. Li, Y. R. Wu, C. D. Medley, Z. H. Cao, J. Li, P. Colon, H. Lin, W. H. Tan, *Angew. Chem. Int. Ed.* **2009**, *48*, 856.
[6] B. Dubertret, M. Calame, A. J. Libchaber, *Nat. Biotechnol.* **2001**, *19*, 365.
[7] F. Li, H. Pei, L. H. Wang, J. X. Lu, J. M. Gao, B. W. Jiang, X. C. Zhao, C. H. Fan, *Adv. Funct. Mater.* **2013**, *23*, 4140.
[8] S. Xu, S. Xu, Y. Zhu, W. Xu, P. Zhou, C. Zhou, B. Dong, H. Song, *Nanoscale* **2014**, *6*, 12573.
[9] Y. J. Guo, L. Deng, J. Li, S. J. Guo, E. K. Wang, S. J. Dong, *ACS Nano* **2011**, *5*, 1282.
[10] Y. J. Song, X. H. Wang, C. Zhao, K. G. Qu, J. S. Ren, X. G. Qu, *Chem. Eur. J.* **2010**, *16*, 3617.
[11] a) D. Sarkar, W. Liu, X. J. Xie, A. C. Anselmo, S. Mitragotri, K. Banerjee, *ACS Nano* **2014**, *8*, 3992; b) Y. Wang, Y. N. Ni, *Anal. Chem.* **2014**, *86*, 7463; c) P. T. K. Loan, W. Zhang, C. T. Lin, K. H. Wei, L. J. Li, C. H. Chen, *Adv. Mater.* **2014**, *26*, 4838.
[12] a) X. M. Zou, J. L. Wang, C. H. Chiu, Y. Wu, X. H. Xiao, C. Z. Jiang, W. W. Wu, L. Q. Mai, T. S. Chen, J. C. Li, J. C. Ho, L. Liao, *Adv. Mater.* **2014**, *26*, 6255; b) R. Cheng, S. Jiang, Y. Chen, Y. Liu, N. Weiss, H. C. Cheng, H. Wu, Y. Huang, X. F. Duan, *Nat. Commun.* **2014**, *5*, 5143.
[13] S. Wi, H. Kim, M. K. Chen, H. Nam, L. J. Guo, E. Meyhofer, X. G. Liang, *ACS Nano* **2014**, *8*, 5270.
[14] E. G. S. Firmiano, A. C. Rabelo, C. J. Dalmaschio, A. N. Pinheiro, E. C. Pereira, W. H. Schreiner, E. R. Leite, *Adv. Energy Mater.* **2014**, *4*, 1301380.
[15] a) M. A. Lukowski, A. S. Daniel, F. Meng, A. Forticaux, L. S. Li, S. Jin, *J. Am. Chem. Soc.* **2013**, *135*. 10274; b) X. Huang, Z. Y. Zeng, S. Y. Bao, M. F. Wang, X. Y. Qi, Z. X. Fan, H. Zhang, *Nat. Commun.* **2013**, *4*, 1444.
[16] a) S. Z. Butler, S. M. Hollen, L. Y. Cao, Y. Cui, J. A. Gupta, H. R. Gutierrez, T. F. Heinz, S. S. Hong, J. X. Huang, A. F. Ismach, E. Johnston-Halperin, M. Kuno, V. V. Plashnitsa, R. D. Robinson, R. S. Ruoff, S. Salahuddin, J. Shan, L. Shi, M. G. Spencer, M. Terrones, W. Windl, J. E. Goldberger, *ACS Nano* **2013**, *7*, 2898; b) Q. H. Wang, K. Kalantar-Zadeh, A. Kis, J. N. Coleman, M. S. Strano, *Nat. Nanotechnol.* **2012**, *7*, 699; c) J. Zheng, H. Zhang, S. Dong, Y. Liu, C. T. Nai, H. S. Shin, H. Y. Jeong, B. Liu, K. P. Loh, *Nat. Commun.* **2014**, *5*, 2995.
[17] a) K. P. Wang, J. Wang, J. T. Fan, M. Lotya, A. O'Neill, D. Fox, Y. Y. Feng, X. Y. Zhang, B. X. Jiang, Q. Z. Zhao, H. Z. Zhang, J. N. Coleman, L. Zhang, W. J. Blau, *ACS Nano* **2013**, *7*, 9260; b) T. B. Wendumu, G. Seifert, T. Lorenz, J.-O. Joswig, A. Enyashin, *J. Phys. Chem. Lett.* **2014**, *5*, 3636; c) Y. C. Wang, J. Z. Ou, S. Balendhran, A. F. Chrimes, M. Mortazavi, D. D. Yao, M. R. Field, K. Latham, V. Bansal, J. R. Friend, S. Zhuiykov, N. V. Medhekar, M. S. Strano, K. Kalantar-zadeh, *ACS Nano* **2013**, *7*, 10083.
[18] a) Y. Hernandez, V. Nicolosi, M. Lotya, F. M. Blighe, Z. Y. Sun, S. De, I. T. McGovern, B. Holland, M. Byrne, Y. K. Gun'ko, J. J. Boland, P. Niraj, G. Duesberg, S. Krishnamurthy, R. Goodhue, J. Hutchison, V. Scardaci, A. C. Ferrari, J. N. Coleman, *Nat. Nanotechnol.* **2008**, *3*, 563; b) J. N. Coleman, M. Lotya, A. O'Neill, S. D. Bergin, P. J. King, U. Khan, K. Young, A. Gaucher, S. De, R. J. Smith, I. V. Shvets, S. K. Arora, G. Stanton, H. Y. Kim, K. Lee, G. T. Kim, G. S. Duesberg, T. Hallam, J. J. Boland, J. J. Wang, J. F. Donegan, J. C. Grunlan, G. Moriarty, A. Shmeliov, R. J. Nicholls, J. M. Perkins, E. M. Grieveson, K. Theuwissen, D. W. McComb, P. D. Nellist, V. Nicolosi, *Science* **2011**, *331*, 568.
[19] R. J. Smith, P. J. King, M. Lotya, C. Wirtz, U. Khan, S. De, A. O'Neill, G. S. Duesberg, J. C. Grunlan, G. Moriarty, J. Chen, J. Wang, A. I. Minett, V. Nicolosi, J. N. Coleman, *Adv. Mater.* **2011**, *23*, 3944.
[20] B. L. Li, L. X. Chen, H. L. Zou, J. L. Lei, H. Q. Luo, N. B. Li, *Nanoscale* **2014**, *6*, 9831.
[21] S. Wang, H. Yu, H. Zhang, A. Wang, M. Zhao, Y. Chen, L. Mei, J. Wang, *Adv. Mater.* **2014**, *26*, 3538.
[22] K. P. Wang, Y. Y. Feng, C. X. Chang, J. X. Zhan, C. W. Wang, Q. Z. Zhao, J. N. Coleman, L. Zhang, W. J. Blau, J. Wang, *Nanoscale* **2014**, *6*, 10530.
[23] K. F. Mark, C. Lee, J. Hone, J. Shan, T. F. Heinz, *Phys. Rev. Lett.* **2010**, *105*, 136805.
[24] D. S. Tsai, K. K. Liu, D. H. Lien, M. L. Tsai, C. F. Kang, C. A. Lin, L. J. Li, J. H. He, *ACS Nano* **2013**, *7*, 3905.
[25] G. Eda, H. Yamaguchi, D. Voiry, T. Fujita, M. Chen, M. Chhowalla, *Nano Lett.* **2011**, *11*, 5111.
[26] B. L. Li, H. Q. Luo, J. L. Lei, N. B. Li, *RSC Adv.* **2014**, *4*, 24256.
[27] H. Li, Q. Zhang, C. C. R. Yap, B. K. Tay, T. H. T. Edwin, A. Olivier, D. Q. Baillargeat, *Adv. Funct. Mater.* **2012**, *22*, 1385.
[28] I. Chowdhury, M. C. Duch, N. D. Mansukhani, M. C. Hersam, D. Bouchard, *Environ. Sci. Technol.* **2013**, *47*, 6288.
[29] a) I. O. Osorio-Roman, A. R. Guerrero, P. Albella, R. F. Aroca, *Anal. Chem.* **2014**, *86*. 10246; b) L. S. Lawson, J. W. Chan, T. Huser, *Nanoscale* **2014**, *6*, 7971.
[30] N. B. Saleh, L. D. Pfefferle, M. Elimelech, *Environ. Sci. Technol.* **2008**, *42*, 7963.
[31] A. Reisch, P. Didier, L. Richert, S. Oncul, Y. Arntz, Y. Mely, A. S. Klymchenko, *Nat. Commun.* **2014**, *5*, 4089.
[32] L. Wu, L. Liu, B. Gao, R. Muñoz-Carpena, M. Zhang, H. Chen, Z. Zhou, H. Wang, *Langmuir* **2013**, *29*, 15174.
[33] A. H. Loo, A. Bonanni, A. Ambrosi, M. Pumera, *Nanoscale* **2014**, *6*, 11971.